OIST OKINAWA INSTITUTE OF SCIENCE AND TECHNOLOGY

Metallic delafossite thin films for unique device applications

メタデータ	言語: English 出版者: AIP Publishing 公開日: 2023-08-30 キーワード (Ja): キーワード (En): 作成者: メールアドレス: 所属:
URL	https://oist.repo.nii.ac.jp/records/2000014

This work is licensed under a Creative Commons Attribution 4.0 International License.

APL Materials

RESEARCH ARTICLE | JULY 19 2022

Metallic delafossite thin films for unique device applications

Special Collection: Materials Challenges and Synthesis Science of Emerging Quantum Materials

Takayuki Harada ; Yoshinori Okada

Check for updates

APL Mater 10, 070902 (2022)
https://doi.org/10.1063/5.0097269
CHORUS

View Online
Export Citation
CrossMark

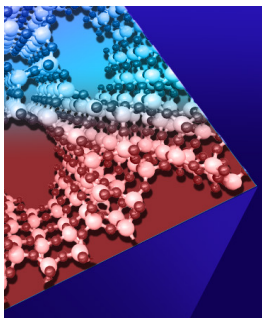

APL Materials
Special Topic:
Open Framework Materials
Submit Today!
AIP Publishing

AIP Publishing

Metallic delafossite thin films for unique device applications

Cite as: APL Mater. 10, 070902 (2022); doi: 10.1063/5.0097269
Submitted: 27 April 2022 • Accepted: 27 June 2022 •
Published Online: 19 July 2022

View Online Export Citation CrossMark

Takayuki Harada[1,2,a] and Yoshinori Okada[3]

AFFILIATIONS

[1] MANA, National Institute for Materials Science, 1-1 Namiki, Tsukuba, Ibaraki 305-0044, Japan
[2] JST, PRESTO, 4-1-8 Honcho, Kawaguchi, Saitama 332-0012, Japan
[3] Quantum Materials Science Unit, Okinawa Institute of Science and Technology (OIST), 1919-1 Tancha, Onna-son, Okinawa 904-0495, Japan

Note: This paper is part of the Special Topic on Materials Challenges and Synthesis Science of Emerging Quantum Materials.
[a] **Author to whom correspondence should be addressed:** HARADA.Takayuki@nims.go.jp

ABSTRACT

Metallic delafossites (ABO_2) are layered oxides with quasi-two-dimensional conduction layers. Metallic delafossites are among the most conducting materials with the in-plane conductivity comparable with that of elemental metals. In this Perspective, we will discuss basic properties and future research prospects of metallic delafossites, mainly focusing on thin films and heterostructures. We exemplify the fascinating properties of these compounds, such as high conductivity and surface polarity, and discuss how it can be utilized in thin films and heterostructures.

© 2022 Author(s). All article content, except where otherwise noted, is licensed under a Creative Commons Attribution (CC BY) license (http://creativecommons.org/licenses/by/4.0/). https://doi.org/10.1063/5.0097269

I. INTRODUCTION

Research on quantum materials has deepened our knowledge of condensed matter physics and expanded the choice of materials for future thin-film devices. Metallic delafossites $PdCoO_2$, $PdCrO_2$, $PdRhO_2$, and $PtCoO_2$, a family of materials that will be the focus of this Perspective, are natural superlattices of two-dimensional (2D) conducting sheets and correlated insulating layers.[1–3] In the rigid oxide framework shown in Fig. 1, metallic delafossites demonstrate intriguing physical properties driven by high electron mobility and surface polarity. These compounds are also chemically inert and thermally stable with a decomposition temperature of ~800 °C or higher in air.[1] The high stability of metallic delafossites gives them great potential for use in thin-film devices.

After an overview of the basic properties of metallic delafossites (Sec. II), this Perspective will focus on two important characteristics of these materials with respect to device applications: high mobility/conductivity, which gives rise to intriguing transport phenomena (Secs. III and IV), and surface polarity, which leads to a large work function and emergent spin polarized surface states (SS) (Secs. V and VI). While high mobility/conductivity and surface polarity are essentially independent properties, metallic delafossites in characteristic layered crystal structures demonstrate these properties. The physical properties of metallic delafossites have mainly been revealed through the study of bulk single crystals[4] with limited research on thin films. For metallic delafossites to be used for device applications, it will be crucial to accelerate research on thin films, which includes making heterostructures by design (Sec. VI). For this purpose, as described in Sec. VII, we emphasize the importance of direct imaging of metallic delafossite thin films using spectroscopic imaging scanning tunneling microscopy (SI-STM).

II. PHYSICAL PROPERTIES OF METALLIC DELAFOSSITES

In this section, a brief overview is given on the physical properties of metallic delafossites. For details, the reader can refer to the existing reviews on single crystals,[4,5] thin films,[6] and theory.[7] As shown in Fig. 1(a), the crystal structure of metallic delafossites consists of ionic layers of A^+ and $[BO_2]^-$ octahedra. Until

© Author(s) 2022

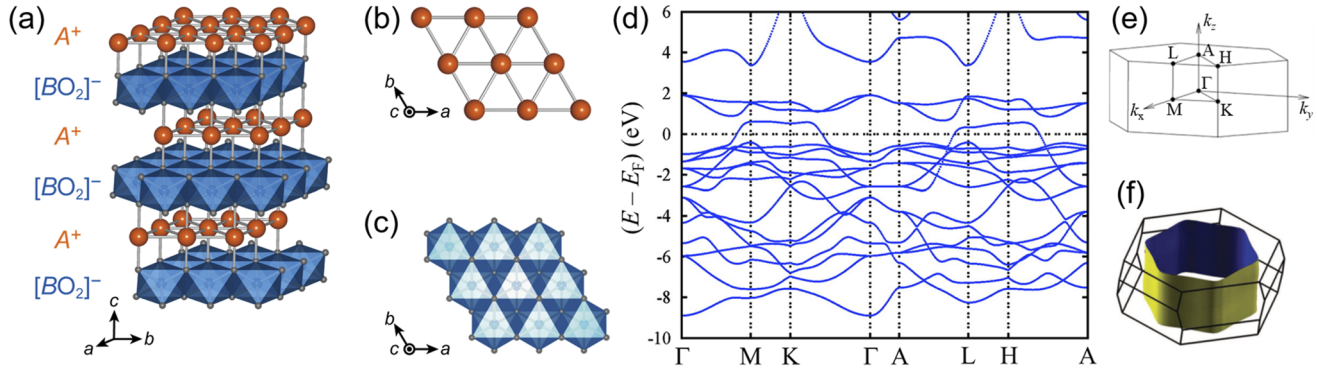

FIG. 1. (a) The crystal structure of metallic delafossites ABO_2. The A^+ and $[BO_2]^-$ layers are noted. (b) The crystal structures of A^+ layers and (c) the $[BO_2]^-$ layers. (d) The electronic band structure, (e) the Brillouin zone of the hexagonal unit cell, and (f) the Fermi surface of $PdCoO_2$ calculated by density functional theory (DFT) in the generalized gradient approximation (GGA). Reprinted with permission from Eyert *et al.*, Chem. Mater. **20**, 2370–2373 (2008). Copyright 2008, American Chemical Society.[79]

now, five compounds in the delafossite family have been shown to exhibit metallic electrical conduction: $PdCoO_2$, $PdCrO_2$, $PdRhO_2$, $PtCoO_2$, and $AgNiO_2$.[4] Here, we will focus on the first four compounds, in which A^+ (Pd^+ or Pt^+) ions mediate electrical conduction, and will refer to them collectively as metallic delafossites. Hereafter, we will not discuss $AgNiO_2$ as in this compound, the *B*-site Ni ions contribute to electrical conduction, resulting in considerably different physical properties from the other four compounds.[8–10]

In each layer, A^+ ions or BO_6 octahedra form 2D triangular lattices [Figs. 1(a)–1(c)]. The A^+ layers are 2D conductive sheets, while the $[BO_2]^-$ layers are insulating in nature. Because of this layered crystal structure, metallic delafossites show quasi-2D electrical conduction. Conductivity in the *ab*-plane (σ_{ab}) of metallic delafossites is generally orders of magnitude higher than along the *c* axis (σ_c). In the case of $PdCoO_2$ at room temperature, $\sigma_{ab} \sim 3.8 \times 10^7$ S/m, while $\sigma_c \sim 9.3 \times 10^4$ S/m. At cryogenic temperatures, the conductivity of $PdCoO_2$ increases by a factor of ~400 for σ_{ab},[11] resulting in an electron mean free path length $l \sim 21.4\ \mu$m.[4,12]

As will be discussed in Sec. III, the quasi-2D high-mobility electrons generate intriguing electrical transport phenomena as recently shown in high-purity single crystals.[13–18] The band structure and Brillouin zone of $PdCoO_2$ are shown in Figs. 1(d) and 1(e). The dispersive band that crosses the Fermi level is predominantly attributed to Pd 4d and Pd 5s states.[19] These electronic states form the nearly cylindrical Fermi surface shown in Fig. 1(f), reflecting the quasi-2D electrons in the Pd layers.

Regarding magnetic properties, $PdCrO_2$ shows antiferromagnetic transition with the Néel temperature $T_N \sim 37.5$ K, while the bulk states of $PdCoO_2$, $PdRhO_2$, and $PtCoO_2$ are nonmagnetic.[4] In $PdCrO_2$, the Cr^{3+} ions have localized spins with $S = 3/2$.[20,21] As shown in Fig. 1(c), the CrO_6 octahedra form geometrically frustrated 2D spin triangular lattices, which influence the high-mobility electrons in the Pd sheets and cause an unconventional anomalous Hall effect.[20] Although $PdCoO_2$, $PdRhO_2$, and $PtCoO_2$ are nonmagnetic in bulk because of the fully occupied t_{2g}-like orbitals, recent experiments have indicated the existence of spin-dependent electronic states at the surface, which will be discussed further in Secs. –V–VII. [22–24]

III. HIGH MOBILITY AND HIGH DENSITY QUASI-2D ELECTRONS

As described in Sec. I, one of the most remarkable characteristics of metallic delafossites is their high electrical conductivity. Figure 2 compares the metallic delafossites and various high-mobility 2D electronic systems: 2D materials, quasi-2D materials, and 2D electrons at surfaces/interfaces [Figs. 2(a)–2(c)]. As shown in Fig. 2(d), currently known high mobility electronic systems have relatively low carrier densities of $n_{2D} < 10^{14}$ cm^{-2}. In contrast, metallic delafossites, plotted in red in Fig. 2(d), are high mobility quasi-2D systems with comparatively high carrier densities of $n_{2D} \sim 10^{15}$ cm^{-2}. Thus, metallic delafossites are unique and ideal for exploring mesoscopic electrical transport phenomena in high mobility, high carrier density materials [Fig. 2(d)].

To compare the cleanness of 2D conduction channels, mean free path l is plotted in Fig. 2(e) for the same set of data as Fig. 2(d). The mean free path of metallic delafossites compares well with most of the high-mobility materials, showing exceptional cleanness of the conduction channels of metallic delafossites [Fig. 2(e)]. As demonstrated by $PdCoO_2$ single crystals at cryogenic temperatures, the 2D electrons in Pd sheets have impressively long electron scattering lengths with an electron mean free path length $l \sim 21.4\ \mu$m[12] and a phase coherence length $l_\phi > 10\ \mu$m.[17] An interesting consequent phenomenon observed for the high-mobility electrons in $PdCoO_2$ is hydrodynamic electron flow.[13] The flow of electrons in solids is normally far different from the hydrodynamic flow of an ordinary fluid like water. In ordinary conductors, electrons are scattered by phonons and impurities, resulting in momentum relaxation and the generation of resistance. On the other hand, if the total momentum of electrons is conserved inside a conductor and is predominantly relaxed at the edges, electrical transport resembles the hydrodynamic motion of a fluid. To achieve this, the rate of momentum-relaxing scattering inside a conductor (electron-impurity, electron–phonon, and Umklapp scattering) should be minimized. In this situation, the channel resistance is partly given by the viscosity of the electron fluid. The viscosity of the electron fluid is governed by the rate of momentum-conserving electron–electron scattering. This was recently demonstrated by Moll *et al.* who

© Author(s) 2022

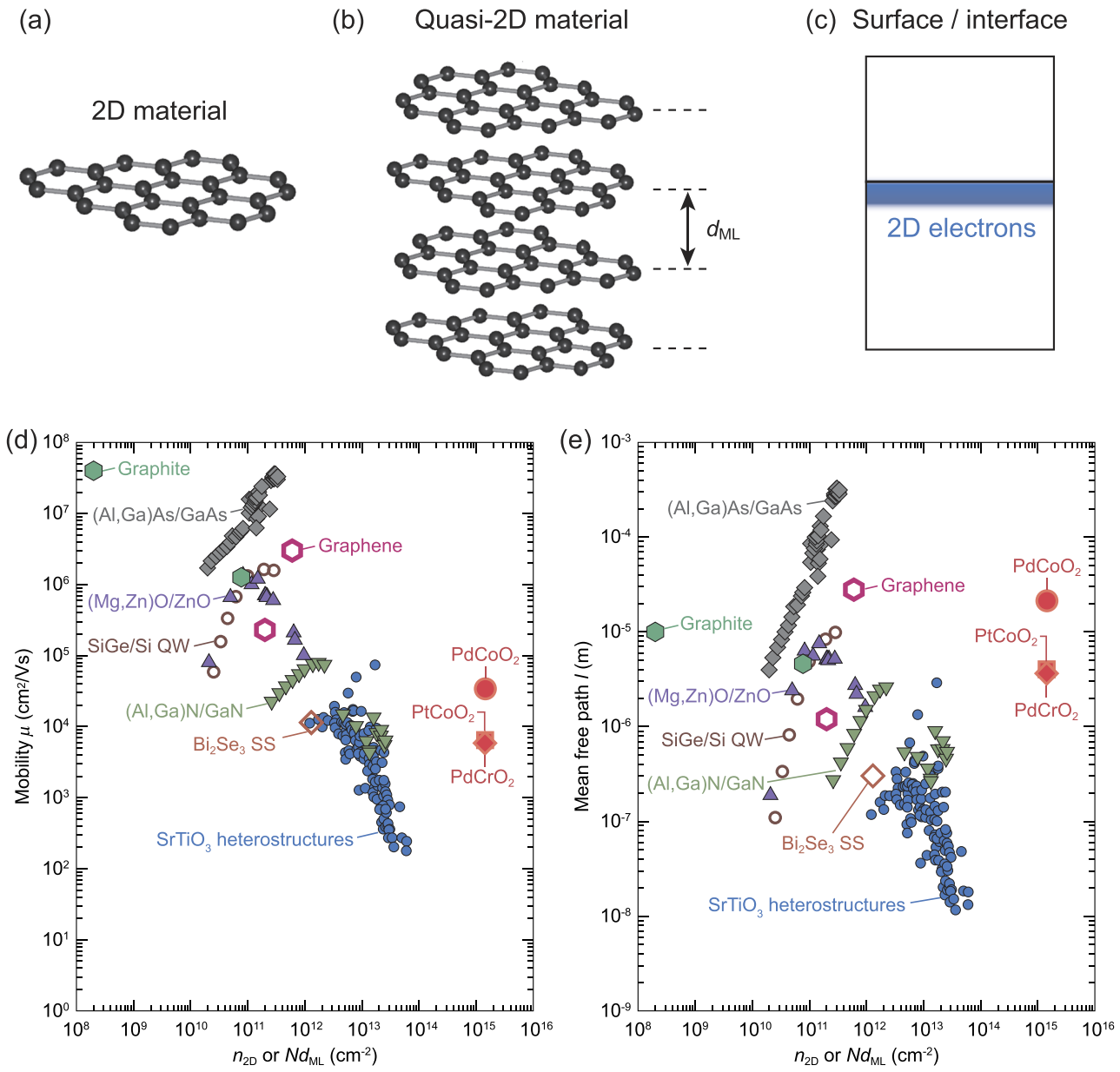

FIG. 2. Comparison of various (quasi-)2D high mobility electronic systems. The schematics of (a) 2D material, (b) quasi-2D material, and (c) 2D electrons at a surface/interface. (d) Charge carrier mobility μ of selected materials. 2D materials: suspended graphene at ~5 K[80] and graphene on h-BN below 130 K (open magenta hexagons).[80,81] Quasi-2D materials: bulk single crystals of $PdCoO_2$ (red circle), $PtCoO_2$ (red square), and $PdCrO_2$ (red diamond) at 4 K[4,12] and graphite (green hexagon) at 4.2[82,83] or 3 K.[84] Semiconductor interfaces: (Al, Ga)As/GaAs heterostructures (black diamonds),[85,86] SiGe/Si quantum wells (QW, brown open circles) at 0.3 K,[87] (Mg, Zn)O/ZnO heterostructures (purple up-pointing triangles) at 500 or ≲100 mK,[88] (Al, Ga)N/GaN heterostructures (green down-pointing triangles) at 20[89] or 0.3 K,[90] and $SrTiO_3$-based heterostructures (blue circles) at low temperatures.[91] Surfaces of topological insulators: the surface states (SS) of Bi_2Se_3 at 1.5 K (light brown open diamond).[92] For the quasi-2D systems, the sheet carrier density for a single conductive layer is calculated as $n_{2D} = Nd_{ML}$ using the carrier concentration N and the interlayer distance d_{ML} schematically shown in (b). The carrier mobility of $PdCoO_2$, $PtCoO_2$, and $PdCrO_2$ is calculated as $\mu = 1/eN\rho$, where e is the elemental charge and ρ is the resistivity. The reported *ab*-plane resistivity is used for ρ. (e) Mean free path l of charge carriers in the same materials as (d). For graphene and graphite, we used the reported values of l in the literature.[80–82,84] For the other materials, the mean free path l is calculated using the formulas for circular Fermi surfaces around valleys: $l = \frac{\hbar k_F \mu}{e}$ and $k_F = \left(\frac{4\pi n_{2D}}{g_s g_v}\right)^{\frac{1}{2}}$, where $\hbar$ is the reduced Planck constant, k_F is the Fermi wave vector, g_s is the spin degeneracy, and g_v is the valley degeneracy. For $SrTiO_3$ heterostructures, the non-circular 2D Fermi surface could result in deviation from the calculated l. We also note that the mean free path is proposed to be limited by the sample size for the graphene data.[80,81]

© Author(s) 2022

fabricated microchannels in $PdCoO_2$ single crystals using a focused ion beam (FIB) technique.[13] The low rate of momentum-relaxing scattering in ultrapure $PdCoO_2$ single crystals results in electrical transport through these microchannels that can be described as hydrodynamic motion.[13,25] Furthermore, various mesoscopic high mobility electrical transport phenomena, such as ballistic[16,18,26] or phase-coherent transport,[17] have been demonstrated in high-purity single crystals of $PdCoO_2$.

Along with the above-mentioned transport phenomena, the high carrier density in metallic delafossites is predicted to cause additional physical effects. Because of the high carrier density, the Fermi surfaces of metallic delafossites are considerably larger than other quasi-2D systems, such as semiconductor heterostructures [Fig. 1(f)]. This can cause the many-body effects, such as quasiparticle formation and/or an anisotropic Fermi surface shape, to appear with the high mobility transport phenomena. For example, because of the large hexagonal cylindrical Fermi surface, the trajectory of ballistic transport is not isotropic as in ordinary 2D systems but highly directional and dominantly oriented in six directions [Figs. 3(a) and 3(b)].[16,18,26] Identifying exotic consequences of many-body effects in mesoscopic electrical transport is an intriguing challenge, which may be facilitated by real-space probing techniques (Sec. VII).

While mesoscopic electrical transport phenomena in metallic delafossites have been mainly studied in FIB-patterned bulk single crystals, these fascinating transport properties are motivating thin-film researchers to grow high-purity $PdCoO_2$ in order to make mesoscopic devices using conventional lithography techniques. Once realized, exotic transport in thin films could be expanded to the study of spin transport or the superconducting proximity effect by making thin-film heterostructures, as will be discussed in Secs. VI and VII. Signatures of phase-coherent transport in $PdCoO_2$ thin films have already been reported in mesoscopic structures.[27] Although l_ϕ and l of thin-film mesoscopic structures are currently

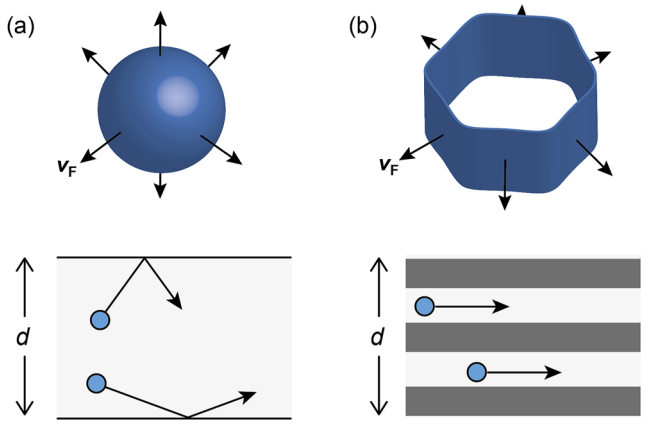

FIG. 3. (a) A spherical Fermi surface (top) and a schematic of electrons traveling with $\boldsymbol{v}_F$ in a thin film with thickness d (bottom). (b) A schematically drawn hexagonal Fermi surface of $PdCoO_2$ (top) and electrons traveling with $\boldsymbol{v}_F$ along the conductive layer of Pd (bottom). The total thickness of the thin film is noted as d. We note that the warping in the $PdCoO_2$ Fermi surface results in a finite component of $\boldsymbol{v}_F$ perpendicular to the conductive layer.

$l_\phi \sim 100$ nm and $l \sim 10$ nm,[27] improving thin film quality could extend these scattering lengths.

IV. TOWARD THIN FILMS WITH HIGH ELECTRON MOBILITY

In this section, we will discuss the possibility of achieving high electron mobility metallic delafossite thin films. Metallic delafossite thin films were first fabricated in the 1980s by annealing amorphous precursors deposited by sputtering.[28] Recently, several groups have reported the fabrication of c axis oriented thin films of $PdCoO_2$,[29–33] $PdCrO_2$,[33–35] and $PtCoO_2$[33] by pulsed laser deposition (PLD),[29,31,34] molecular beam epitaxy,[30,32] and solution-based processes.[33]

Is it possible to increase the electron mobility of thin films to the level of single crystals? With the exception of metallic delafossites, studies on the resistivity of thin metal films have a long history. Studies on elemental metals, such as Au,[36] Pt,[37] Co,[38] and Cu,[39,40] have shown that the resistivity of metals scales with thin film thickness and generally increases as the thickness is reduced down to a few nanometers, which can be explained by the surface scattering of electrons. According to theory, the resistivity, ρ, of three-dimensional metals is expected to increase as the thickness, d, decreases, with $\rho \propto 1/[d\ln(l_{bulk}/d)]$,[41,42] $\rho \propto 1/d$,[40] or $\rho \propto 1/d^2$,[43–45] depending on the model, where l_{bulk} is the bulk mean free path.

Because of the quasi-2D nature of $PdCoO_2$, a reduction in thickness may not cause a serious surface scattering effect since electron mobility could be maintained, as seen in other quasi-2D systems like graphite. The directional transport effect found in single crystals of $PdCoO_2$ is an encouraging result that supports this hypothesis. According to transport measurements of $PdCoO_2$ single crystals,[16,18,26] the ballistic transport of electrons is highly anisotropic, reflecting the hexagonal cylindrical shape of the Fermi surface. The spherical Fermi surfaces of alkali metals are compared with those of $PdCoO_2$ in Figs. 3(a) and 3(b).

The velocity of electrons, $\boldsymbol{v}_n$, is expressed as

$$\boldsymbol{v}_n(\boldsymbol{k}) = \frac{1}{\hbar}\nabla_{\boldsymbol{k}}\varepsilon_n(\boldsymbol{k}),$$

where n is the band index, $\boldsymbol{k}$ is the wavevector, $\hbar$ is the reduced Planck constant, and $\varepsilon_n(\boldsymbol{k})$ is the energy of an electron with $\boldsymbol{k}$ in the nth band.[46] The Fermi velocity, $\boldsymbol{v}_F$, is, therefore, perpendicular to the Fermi surface and is isotropic in alkali metals that have additional one electron to the closed-shell configuration. In contrast, $\boldsymbol{v}_F$ of $PdCoO_2$ is dominantly oriented in six directions in the ab-plane (Fig. 3, top). Because of the directional ballistic transport, c axis oriented thin films of metallic delafossites may not be significantly affected by surface scattering (Fig. 3, bottom). Although the warping in the Fermi surface of $PdCoO_2$ causes a finite out-of-plane component of $\boldsymbol{v}_F$ and sets a limitation to the above discussion,[47] the nearly cylindrical Fermi surface of $PdCoO_2$ should be a predominant advantage for achieving a long mean free path in thin films.

Table I summarizes the challenges toward high-mobility thin films of metallic delafossites and reported approaches. So far, $PdCoO_2$ has been most studied for thin films among the metallic delafossites. The typical growth condition of $PdCoO_2$ for PLD is the substrate temperature of 620–700 °C and the oxygen pressure

© Author(s) 2022

TABLE I. Challenges in growth and processing of metallic delafossite thin films and tested approach.

Growth/processing challenges	Tested approach	Applied materials
Twinning	Miscut substrates[31]	$PdCoO_2$
	Substrates with low symmetry surfaces	
	β-Ga_2O_3 (−201)[55]	$PdCoO_2$ and $PdCrO_2$
	$SrTiO_3$ (111)[34,49]	$PdCrO_2$
	Buffer layers: $CuCrO_2$[34,49]	$PdCrO_2$
	Delafossite-type substrates: $CuFeO_2$[48]	⋯
Stacking faults	Observed by HAADF-STEM[27,30]	$PdCoO_2$
Impurities	PLD with high purity targets ($PdCoO_2$ 4N5 and Pd 5N)[50]	$PdCoO_2$
	MBE with high purity sources (Pd 5N and Co 4N5)[32]	$PdCoO_2$
Cation stoichiometry	Alternate ablation of $PdCoO_2$ and PdO_x in PLD[29]	$PdCoO_2$
	MBE growth[30,32]	$PdCoO_2$
Oxygen vacancies	Post-annealing in air or O_2 improves *RRR*[30]	$PdCoO_2$
	MBE in atomic oxygen plasma[30] or ozone[32]	$PdCoO_2$
Atomic ordering	Post-annealing in air or O_2 improves *RRR*[30]	$PdCoO_2$
	Chemical growth method	
	Solution-based growth[33]	$PdCoO_2$, $PdCrO_2$, and $PtCoO_2$
	Atomic layer deposition[51]	$PtCoO_2$
Lattice matching (*ab*-plane and *c* axis)	Buffer layers: $CuCrO_2$[34,49]	$PdCrO_2$
	Delafossite-type substrates: $CuFeO_2$[48]	⋯
Wide area	Solution-based growth on 2-in. wafers[33]	$PdCoO_2$, $PdCrO_2$, and $PtCoO_2$
Heterostructures	Schottky junctions with β-Ga_2O_3[35,55–57]	$PdCoO_2$ and $PdCrO_2$
Microfabrication	Electron beam lithography and Ar ion milling[27]	$PdCoO_2$
	Resist: HSQ and linewidth: ~100 nm	

of 0.1–1.7 Torr.[29,31] For MBE growth, the substrate temperature ranges from 300 to 480 °C under atomic oxygen plasma[30] or distilled ozone.[32] The room-temperature *ab*-plane resistivity ρ_{ab} of the $PdCoO_2$ thin films reported to date is about two to five times higher than that of the bulk single crystal (ρ_{ab} = 2.6 $\mu\Omega$ cm).[6,29] The low-temperature resistivity has been reported for these thin films. The largest residual resistivity ratio (*RRR*) for $PdCoO_2$ of 16 has been reported in a thick (~180 nm) MBE-grown $PdCoO_2$ thin film that is post-annealed at 800 °C in oxygen.[30] The *RRR* of 16 in the $PdCoO_2$ thin film is still small compared with the bulk value (*RRR* ~ 400).[11]

To improve the thin-film quality, dominant scattering sources should be clarified. One of the possible dominant scattering sources is twin boundaries. For *c* axis oriented thin-film growth of metallic delafossites, Al_2O_3 substrates are widely used. As the surface of Al_2O_3 substrates is effectively sixfold symmetric, the reported thin films have crystal twins that are 180°-rotated from each other.[29,30,32] These twin boundaries can scatter electrons. Growing single crystal thin films without twin boundaries could dramatically improve electron mobility. Although various promising approaches, as listed in Table I, to achieve this using single crystal substrates with delafossite structures[48] or twin-free delafossite buffer layers[49] have been reported, twin-free thin films have not been realized. Toward twin-free thin films, stacking faults need to be also suppressed.

Other possible scattering sources include point defects caused by impurities, cation off stoichiometry, and oxygen vacancies. As the *RRR* of thin films has not been significantly dependent on the purity of the material sources (PLD targets and MBE sources),[32,50] impurity scattering seems not a dominant scattering mechanism in the current metallic delafossite thin films. The increase in *RRR* by post-annealing could be due to the reduction of oxygen vacancies as well as improved atomic ordering in the crystal. The post-annealing temperature is limited by the decomposition temperature of metallic delafossites (800–925 °C). Alternative approaches, such as thin-film growth techniques, based on chemical reactions could be promising to improve atomic ordering as they may mimic the bulk synthesis of pure single crystals.[33,51]

As a potentially low-cost and wide-area deposition technique that is important for application, solution-based growth on 2-in. wafers has been reported for $PdCoO_2$, $PdCrO_2$, and $PtCoO_2$.[33] Regarding device fabrication, $PdCoO_2$ has been successfully patterned into submicrometer scales by conventional electron beam lithography and Ar-ion milling.[27] As discussed in Secs. V and VI, search for novel heterostructures is important to find a possible application of metallic delafossites.

© Author(s) 2022

V. POLAR SURFACES FOR DEVICE APPLICATIONS

Along with high electron mobility/conductivity, the surface polarity of metallic delafossites is also highly significant as it permits an exceptionally large work function, which is beneficial for device applications. According to the classification by Tasker,[52] the *c*-plane surfaces of metallic delafossites are classified as type-3 polar surfaces.[6] As a result, the surface properties of metallic delafossites strongly depend on the termination layer of the surface (e.g., Pd or CoO_2 layer). Recent surface measurements of cleaved $PdCoO_2$ showed that the work function of a Pd-terminated surface (ϕ_m^{Pd}) was ~4.7 eV, while a CoO_2-terminated surface (ϕ_m^{CoO2}) was ~7.8 eV, indicating that the work function of $PdCoO_2$ is highly dependent on the termination layer.[53] The large difference between ϕ_m^{Pd} and ϕ_m^{CoO2} is due to the polar surface. A work function of ~7.8 eV is very large for a metallic compound and far exceeds the Pt work function (~5.65 eV), which is the largest value found in elemental metals.[54]

The large work function of $PdCoO_2$ should be of great value for various device applications, such as for electrodes for semiconductor devices. In Fig. 4, the work function of $PdCoO_2$ (ϕ_m^{Pd} and ϕ_m^{CoO2}) is compared with the conduction band minimum (CBM) and valence band maximum (VBM) of various semiconductors. In semiconductor devices, Schottky junctions formed at metal/semiconductor interfaces often play key roles in device operation. According to the Schottky–Mott relationship, the ideal Schottky barrier height of metal/n-type semiconductor interfaces, $\phi_{b,n}$, is estimated to be $\phi_{b,n} = \phi_m - \chi$, where ϕ_m is the work function of a metal and χ is the electron affinity of a semiconductor. As shown in Fig. 4, the difference between ϕ_m^{CoO2} and χ of various semiconductors is as large as several eV. Therefore, large Schottky barrier heights can be achieved in $PdCoO_2$/n-type semiconductor polar interfaces, as demonstrated by $PdCoO_2/\beta$-Ga_2O_3[55–57] and $PdCrO_2/\beta$-Ga_2O_3 junctions.[35] The large Schottky barrier height would be useful for diodes for high-temperature operation and Schottky gates for transistors. Careful control of the initial growth layer would be important to generate an interface with a homogeneous Schottky barrier height.

In general, ohmic contacts with low contact resistance are important to reduce power loss in wide bandgap semiconductor

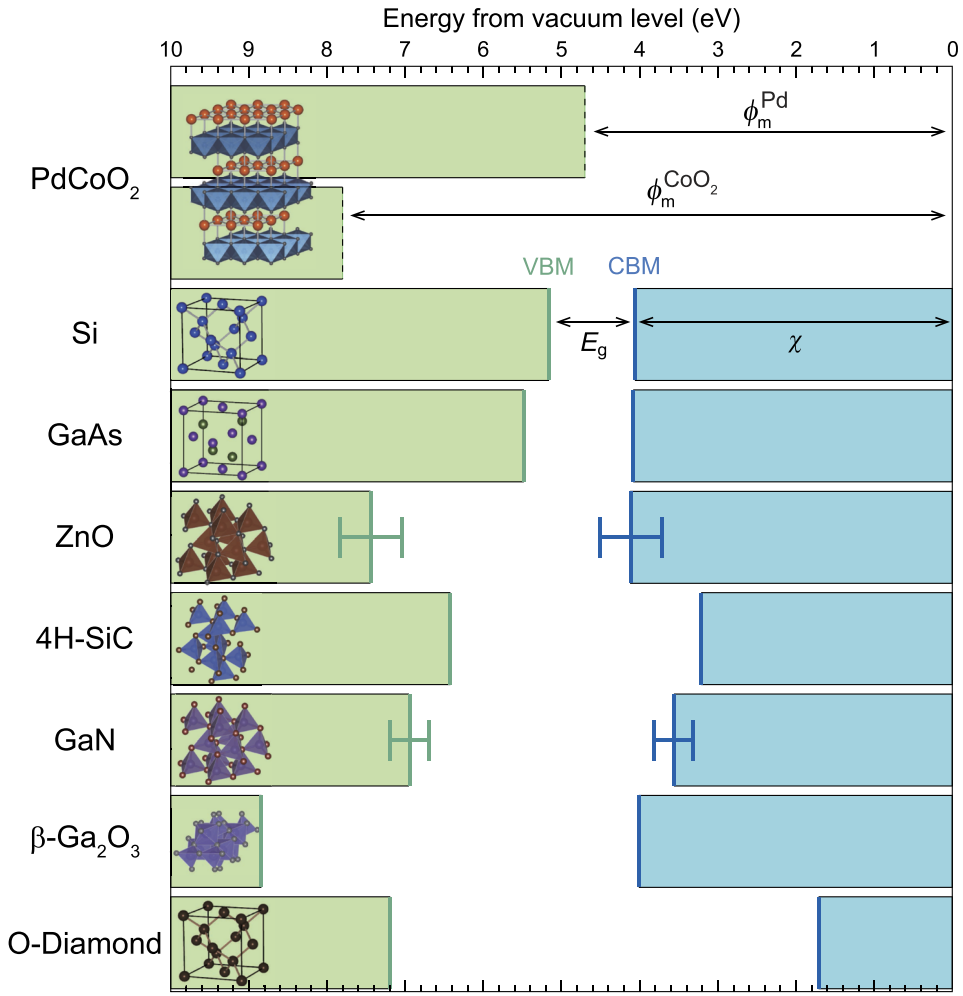

FIG. 4. The band alignment of semiconductors compared with the work function of Pd-terminated (ϕ_m^{Pd})[53,55] and CoO_2-terminated (ϕ_m^{CoO2})[53] $PdCoO_2$. The valence and conduction bands of various semiconductors are shown in green and blue, respectively. For Si, the electron affinity (χ), the bandgap (E_g), the conduction band minimum (CBM), and the valence band maximum (VBM) are noted. The band alignment is drawn based on the reported bandgap and the electron affinity for Si,[93] GaAs,[93] ZnO,[93,94] 4H–SiC,[95] GaN,[96] β-Ga_2O_3,[97,98] and oxidized diamond surfaces.[99,100] For ZnO and GaN, the CBM and VBM are shown with bars, which are reported to depend on the surface termination.[94,96]

© Author(s) 2022

devices. Making low resistance contacts to p-type wide bandgap semiconductors is often a challenge, particularly when the hole concentration is low. In the Schottky–Mott relationship, the Schottky barrier height of a metal/p-type semiconductor interface is $\phi_{b,p} = \chi + E_g - \phi_m$, where E_g is the bandgap of the semiconductor. To achieve a true ohmic contact ($\phi_{b,p} < 0$), one needs a metal with $\phi_m > \chi + E_g$. For wide bandgap semiconductors, such as 4H–SiC ($E_g \sim 3.2$ eV) and GaN ($E_g \sim 3.4$ eV), $\chi + E_g$ is well above 6 eV, and there is no elemental metal electrode that satisfies $\phi_m > \chi + E_g$. As shown in Fig. 4, $PdCoO_2$ with a CoO_2 initial layer is a promising candidate for a true ohmic contact for wide bandgap semiconductors since ϕ_m^{CoO2} is larger than $\chi + E_g$ of semiconductors with p-type doping (Si, GaAs, ZnO, 4H–SiC, GaN, and diamond).

VI. SURFACE SPIN STATES

Surface polarity also causes emergent spin polarized surface states. In general, to electrostatically stabilize the polar surface, charge compensation occurs.[52,58,59] This causes the electron density at the surface to differ from that of the inner bulk. Recent experiments have indicated that charge compensation changes the surface of the inherently nonmagnetic $PdCoO_2$ to have spin-dependent electronic states.

The surface electronic states of $PdCoO_2$ have been calculated using a density functional theory (DFT)-based method.[60] Owing to the electronic reconstruction induced by the surface polarity, a Pd-terminated surface of $PdCoO_2$ was proposed to have surface magnetism.[60] The calculation also predicted that the Co-derived bands at a CoO_2-terminated surface are split because of the spin–orbit interaction.[60]

Sunko *et al.* observed the BO_2-terminated surfaces of $PdCoO_2$, $PtCoO_2$, and $PdRhO_2$ by angle-resolved photoemission spectroscopy (ARPES) and discovered Rashba-like spin splitting,[22] which is caused by strong inversion symmetry breaking on the BO_2-terminated surface. Spin splitting is comparable to atomic spin–orbit coupling (SOC) of *B*-site cations. Mazzola *et al.* reported the surface ferromagnetic states at Pd-terminated surfaces of $PdCoO_2$ by ARPES.[23] Ferromagnetism has also been detected in PLD-grown $PdCoO_2$ thin films by ARPES and the anomalous Hall effect.[24] From the magnetoresistance measurements under the in-plane magnetic field, the Pd-terminated surface of $PdCoO_2$ also has Rashba-spin splitting with a Rashba coefficient of ~0.75 ± 0.3 eV.[61] Possible coexistence of ferromagnetism and Rashba spin–orbit coupling will be an interesting subject for future studies in the context of spin-orbitronics.[62]

Here, we will discuss the prospects of using the Rashba ferromagnetic surfaces of metallic delafossites. We performed DFT calculations of a Pt-terminated $PtCoO_2$ surface (Fig. 5) and found similar properties to that of $PdCoO_2$. In the nonmagnetic calculation, Rashba-like split bands were observed around the Γ point. Furthermore, the flat region of the conduction band shifted close to the Fermi level, which may cause Stoner splitting, as with $PdCoO_2$.[23] In the calculation considering collinear spin polarization, the bands around the Γ point were spin-split. The Rashba effect visible in the nonmagnetic calculation was more pronounced in $PtCoO_2$ compared with that in $PdCoO_2$ because of the larger atomic spin–orbit coupling in Pt than in Pd [Fig. 5(a)].

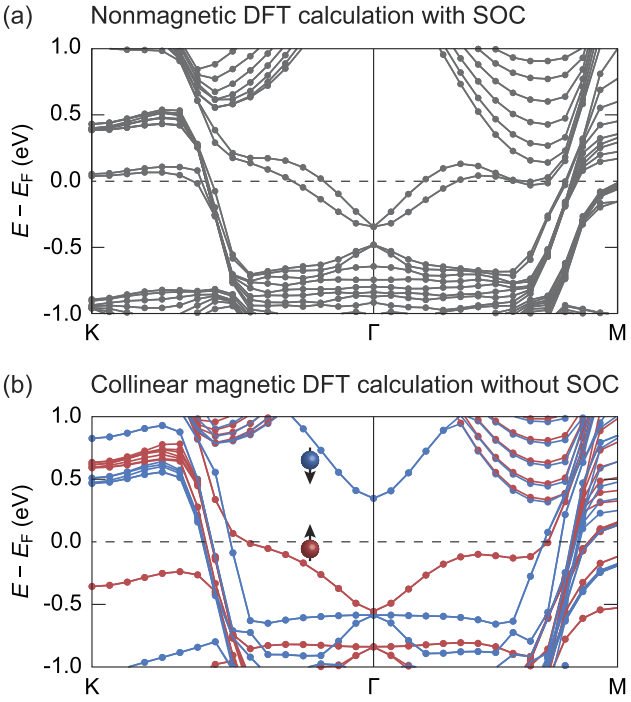

FIG. 5. The electronic structure of the slab model for a Pt-terminated $PtCoO_2$, calculated by density functional theory (DFT) using the CASTEP package. The vertical axis is the energy relative to the Fermi level (E_F). (a) The nonmagnetic calculation result considering spin–orbit coupling (SOC). (b) The calculation result considering collinear spin-polarization. The red and blue lines correspond to the spin-up and spin-down states, respectively. For (b), SOC is not included because of the limitation of our computer setup. Including spin–orbit interaction can give rise to non-collinear spin textures and require larger supercells for calculation. A symmetric slab model containing nine Pt and eight CoO_2 layers with a vacuum gap of 15 Å is employed for the calculation following a report on $PdCoO_2$.[23] The inner five Pt and four CoO_2 layers are fixed to have the lattice constants of bulk single crystals.[4] The outer four Pt and four CoO_2 layers were relaxed. For both (a) and (b), the generalized gradient approximation and Perdew–Burke–Ernzerhof (GGA-PBE) functionals are used, and the Hubbard *U* is not taken into account.

Surface spin-split electronic states can be utilized in heterostructures to induce exotic electronic states. For example, making a heterostructure with a superconductor may be interesting. As a model system that could show topological superconductivity, a 2D electronic system with relatively large spin–orbit coupling, effective Zeeman coupling, and proximity-induced superconductivity has been proposed.[63,64] The model Hamiltonian can be written as $H(k) = H_0(k) + H_R(k) + H_Z + H_S$, where H_0 is the kinetic energy, H_R is the Rashba spin–orbit interaction, H_Z is the effective Zeeman interaction, and H_S is the spin-singlet s-wave pair potential.[64] At the surface of $PtCoO_2$ or $PdCoO_2$, there can be a relatively large spin–orbit coupling $H_R(k)$ and Stoner splitting (i.e., effective Zeeman coupling, H_Z) in a nearly 2D conduction channel. Inducing superconductivity H_S by the proximity effect and applying a magnetic field to adjust H_Z might induce topological superconducting states.

© Author(s) 2022

VII. REAL SPACE PROBING OF ELECTRONIC STATES

To search for exotic electronic states in metallic delafossites, it is important to understand the external magnetic field dependence of electronic states. An ideal experimental approach for this purpose is SI-STM, which has a unique capability to resolve differential conductance [$dI/dV(r,E,B)$] that is proportional to the density of state below and above E_F, as a function of position r with atomic precision, energy E, and magnetic field B.[65–70] SI-STM has been applied to the polar surfaces of $PdCoO_2$ bulk single crystals. On CoO_2-terminated surfaces of $PdCoO_2$, long-lived quasiparticle states have been visualized as extended six-fold standing waves.[53] This observation is consistent with the anisotropic hexagonal cylindrical Fermi surface of high mobility electrons [Fig. 3(b)]. The observed standing waves have been interpreted by considering the large Rashba-like band splitting driven by strong inversion symmetry breaking.[53] On Pd-terminated surfaces of $PdCoO_2$, SI-STM has revealed the formation of charge density waves[71] and renormalized electronic states that are coupled with magnons.[72]

To further understand the electronic states of $PdCoO_2$ surfaces, SI-STM under external magnetic fields would be informative. As discussed in Sec. VI, metallic delafossites are expected to contain characteristic surface spin states. On Pd-terminated surfaces of $PdCoO_2$ (and possibly in $PtCoO_2$), the possible coexistence of H_R and H_Z may give rise to spin-momentum coupled electronic structures with a H_Z-derived gap at the band crossing point (Fig. 5). Such spin-momentum coupled band structures with surface ferromagnetism could respond to external magnetic fields with controlled magnitude and direction.[73,74] For example, studies on magnetic field dependent standing wave patterns and spatially averaged $dI/dV(E)$ shapes could reveal the spin-momentum coupled states of $PdCoO_2$. As SI-STM can visualize spin texture with atomic resolution in real space,[75–78] searching for topological magnetism on the surface of metallic delafossites is an exciting prospect.

To the best of our knowledge, all SI-STM studies reported to date were performed on cleaved surfaces of single crystals. By applying SI-STM to metallic delafossite thin films (Fig. 6), we would be able to investigate the electronic states of heterostructures with other materials, such as the superconductors discussed in Sec. VI. Furthermore, as with other layered materials, monolayer-thick metallic delafossites may also be an interesting system for SI-STM study.

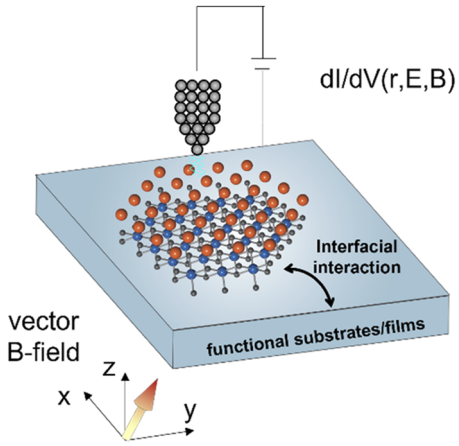

FIG. 6. A conceptual figure for spectroscopic imaging scanning tunneling microscopy (SI-STM) on metallic delafossite thin films and heterostructures. SI-STM is able to visualize electronic states with ultra-high spatial and energy resolution under controlled external magnetic fields.

Finally, another important task is to identify the scattering sources that limit the electron mobility of thin films. The electronic scattering response to twin-domain boundaries and point defects could be visualized by SI-STM, which would provide feedback for thin-film growth optimization. The combination of thin-film growth and real-space imaging techniques may lead to high-mobility thin films, facilitating research into unexplored phenomena in ultrathin films and heterostructures.

VIII. CONCLUSION

In this Perspective, we have provided an overview of the physical properties of metallic delafossites and discussed the perspectives of thin-film research. Inherent high mobility and surface polarity make metallic delafossites fascinating materials for both basic and application studies. In particular, mesoscopic electrical transport, many-body effects derived from fermiology, and the interplay of these may lead to intriguing unexplored phenomena. Thin film growth of metallic delafossites would provide tremendous research possibilities for the design of heterostructures and functional devices.

ACKNOWLEDGMENTS

The authors would like to thank Professor A. Tsukazaki and all collaborators for their contributions to this work on metallic delafossites. This work was supported by a Grant-in-Aid for Scientific Research (B) (Grant No. 20H02611), a Grant-in-Aid for Challenging Research (exploratory) (Grant No. 20K21138) from the Japan Society for the Promotion of Science (JSPS), MEXT Leading Initiative for Excellent Young Researchers (Grant No. JPMXS0320200047), JST PRESTO (Grant No. JPMJPR20AD), the Izumi Science and Technology Foundation, and the Foundation for The Promotion of Ion Engineering.

AUTHOR DECLARATIONS

Conflict of Interest

The authors have no conflicts to disclose.

Author Contributions

Takayuki Harada: Conceptualization (lead); Data curation; Formal analysis; Writing - original draft; Writing - review & editing. **Yoshinori Okada:** Conceptualization (supporting); Data curation (equal); Formal analysis (equal); Writing – original draft (supporting); Writing – review & editing (supporting).

DATA AVAILABILITY

The data that support the findings of this study are available from the corresponding author upon reasonable request.

© Author(s) 2022

REFERENCES

[1] R. D. Shannon, D. B. Rogers, and C. T. Prewitt, Inorg. Chem. **10**, 713–718 (1971).
[2] R. D. Shannon, C. T. Prewitt, and D. B. Rogers, Inorg. Chem. **10**, 719–723 (1971).
[3] R. D. Shannon, D. B. Rogers, C. T. Prewitt, and J. L. Gillson, Inorg. Chem. **10**, 723–727 (1971).
[4] A. P. Mackenzie, Rep. Prog. Phys. **80**, 032501 (2017).
[5] R. Daou, R. Frésard, V. Eyert, S. Hébert, and A. Maignan, Sci. Technol. Adv. Mater. **18**, 919–938 (2017).
[6] T. Harada, Mater. Today Adv. **11**, 100146 (2021).
[7] F. Lechermann, npj Comput. Mater. **7**, 120 (2021).
[8] Y. J. Shin, J. P. Doumerc, P. Dordor, C. Delmas, M. Pouchard, and P. Hagenmuller, J. Solid State Chem. **107**, 303–313 (1993).
[9] A. I. Coldea, A. Carrington, R. Coldea, L. Malone, A. F. Bangura, M. D. Johannes, I. I. Mazin, E. A. Yelland, J. G. Analytis, J. A. A. J. Perenboom, C. Jaudet, D. Vignolles, T. Sorgel, and M. Jansen, arXiv:0908.4169 (2009).
[10] A. I. Coldea, L. Seabra, A. McCollam, A. Carrington, L. Malone, A. F. Bangura, D. Vignolles, P. G. van Rhee, R. D. McDonald, T. Sorgel, M. Jansen, N. Shannon, and R. Coldea, Phys. Rev. B **90**, 020401 (2014).
[11] H. Takatsu, S. Yonezawa, S. Mouri, S. Nakatsuji, K. Tanaka, and Y. Maeno, J. Phys. Soc. Jpn. **76**, 104701 (2007).
[12] C. W. Hicks, A. S. Gibbs, A. P. Mackenzie, H. Takatsu, Y. Maeno, and E. A. Yelland, Phys. Rev. Lett. **109**, 116401 (2012).
[13] P. J. W. Moll, P. Kushwaha, N. Nandi, B. Schmidt, and A. P. Mackenzie, Science **351**, 1061–1064 (2016).
[14] N. Kikugawa, P. Goswami, A. Kiswandhi, E. S. Choi, D. Graf, R. E. Baumbach, J. S. Brooks, K. Sugii, Y. Iida, M. Nishio, S. Uji, T. Terashima, P. M. C. Rourke, N. E. Hussey, H. Takatsu, S. Yonezawa, Y. Maeno, and L. Balicas, Nat. Commun. **7**, 010903 (2016).
[15] N. Nandi, T. Scaffidi, P. Kushwaha, S. Khim, M. E. Barber, V. Sunko, F. Mazzola, P. D. C. King, H. Rosner, P. J. W. Moll, M. König, J. E. Moore, S. Hartnoll, and A. P. Mackenzie, npj Quantum Mater. **3**, 66 (2018).
[16] M. D. Bachmann, A. L. Sharpe, A. W. Barnard, C. Putzke, M. König, S. Khim, D. Goldhaber-Gordon, A. P. Mackenzie, and P. J. W. Moll, Nat. Commun. **10**, 5081 (2019).
[17] C. Putzke, M. D. Bachmann, P. McGuinness, E. Zhakina, V. Sunko, M. Konczykowski, T. Oka, R. Moessner, A. Stern, M. König, S. Khim, A. P. Mackenzie, and P. J. W. Moll, Science **368**, 1234–1238 (2020).
[18] P. H. McGuinness, E. Zhakina, M. König, M. D. Bachmann, C. Putzke, P. J. W. Moll, S. Khim, and A. P. Mackenzie, Proc. Natl. Acad. Sci. U.S.A. **118**, e2113185118 (2021).
[19] M. Tanaka, M. Hasegawa, T. Higuchi, T. Tsukamoto, Y. Tezuka, S. Shin, and H. Takei, Physica B **245**, 157–163 (1998).
[20] H. Takatsu, S. Yonezawa, S. Fujimoto, and Y. Maeno, Phys. Rev. Lett. **105**, 137201 (2010).
[21] H. Takatsu, G. Nénert, H. Kadowaki, H. Yoshizawa, M. Enderle, S. Yonezawa, Y. Maeno, J. Kim, N. Tsuji, M. Takata, Y. Zhao, M. Green, and C. Broholm, Phys. Rev. B **89**, 104408 (2014).
[22] V. Sunko, H. Rosner, P. Kushwaha, S. Khim, F. Mazzola, L. Bawden, O. J. Clark, J. M. Riley, D. Kasinathan, M. W. Haverkort, T. K. Kim, M. Hoesch, J. Fujii, I. Vobornik, A. P. Mackenzie, and P. D. C. King, Nature **549**, 492–496 (2017).
[23] F. Mazzola, V. Sunko, S. Khim, H. Rosner, P. kushwaha, O. J. Clark, L. Bawden, I. Marković, T. K. Kim, M. Hoesch, A. P. Mackenzie, and P. D. C. King, Proc. Natl. Acad. Sci. U. S. A. **115**, 12956–12960 (2018).
[24] T. Harada, K. Sugawara, K. Fujiwara, M. Kitamura, S. Ito, T. Nojima, K. Horiba, H. Kumigashira, T. Takahashi, T. Sato, and A. Tsukazaki, Phys. Rev. Res. **2**, 013282 (2020).
[25] G. Varnavides, Y. Wang, P. J. W. Moll, P. Anikeeva, and P. Narang, Phys. Rev. Mater. **6**, 045002 (2022).
[26] M. D. Bachmann, A. L. Sharpe, G. Baker, A. W. Barnard, C. Putzke, T. Scaffidi, N. Nandi, P. H. McGuinness, E. Zhakina, M. Moravec, S. Khim, M. König, D. Goldhaber-Gordon, D. A. Bonn, A. P. Mackenzie, and P. J. W. Moll, Nat. Phys. (published online, 2022).
[27] T. Harada, P. Bredol, H. Inoue, S. Ito, J. Mannhart, and A. Tsukazaki, Phys. Rev. B **103**, 045123 (2021).
[28] P. F. Carcia, R. D. Shannon, P. E. Bierstedt, and R. B. Flippen, J. Electrochem. Soc. **127**, 1974–1980 (1980).
[29] T. Harada, K. Fujiwara, and A. Tsukazaki, APL Mater. **6**, 046107 (2018).
[30] M. Brahlek, G. Rimal, J. M. Ok, D. Mukherjee, A. R. Mazza, Q. Lu, H. N. Lee, T. Z. Ward, R. R. Unocic, G. Eres, and S. Oh, Phys. Rev. Mater. **3**, 093401 (2019).
[31] P. Yordanov, W. Sigle, P. Kaya, M. E. Gruner, R. Pentcheva, B. Keimer, and H.-U. Habermeier, Phys. Rev. Mater. **3**, 085403 (2019).
[32] J. Sun, M. R. Barone, C. S. Chang, M. E. Holtz, H. Paik, J. Schubert, D. A. Muller, and D. G. Schlom, APL Mater. **7**, 121112 (2019).
[33] R. Wei, P. Gong, M. Zhao, H. Tong, X. Tang, L. Hu, J. Yang, W. Song, X. Zhu, and Y. Sun, Adv. Funct. Mater. **30**, 2002375 (2020).
[34] J. M. Ok, M. Brahlek, W. S. Choi, K. M. Roccapriore, M. F. Chisholm, S. Kim, C. Sohn, E. Skoropata, S. Yoon, J. S. Kim, and H. N. Lee, APL Mater. **8**, 051104 (2020).
[35] T. Miyakawa, T. Harada, S. Ito, and A. Tsukazaki, J. Appl. Phys. **128**, 025302 (2020).
[36] G. Kästle, H.-G. Boyen, A. Schröder, A. Plettl, and P. Ziemann, Phys. Rev. B **70**, 165414 (2004).
[37] H. Hoffmann and G. Fischer, Thin Solid Films **36**, 25–28 (1976).
[38] E. Milosevic, S. Kerdsongpanya, M. E. McGahay, A. Zangiabadi, K. Barmak, and D. Gall, J. Appl. Phys. **125**, 245105 (2019).
[39] H.-D. Liu, Y.-P. Zhao, G. Ramanath, S. P. Murarka, and G.-C. Wang, Thin Solid Films **384**, 151–156 (2001).
[40] T. Zhou and D. Gall, Phys. Rev. B **97**, 165406 (2018).
[41] K. Fuchs, Math. Proc. Cambridge Philos. Soc. **34**, 100–108 (1938).
[42] E. H. Sondheimer, Adv. Phys. **1**, 1 (1952).
[43] Z. Tešanović, M. V. Jarić, and S. Maekawa, Phys. Rev. Lett. **57**, 2760–2763 (1986).
[44] N. Trivedi and N. W. Ashcroft, Phys. Rev. B **38**, 012298 (1988).
[45] D. Calecki, Phys. Rev. B **42**, 6906–6915 (1990).
[46] N. W. Ashcroft and N. D. Mermin, *Solid State Physics* (Saunders College Publishing, PA, 1976).
[47] G. Baker, T. W. Branch, J. Day, D. Valentinis, M. Oudah, P. McGuinness, S. Khim, P. Surówka, R. Moessner, J. Schmalian, A. P. Mackenzie, and D. A. Bonn, arXiv:2204.14239 (2022).
[48] N. Wolff, T. Schwaigert, D. Siche, D. G. Schlom, and D. Klimm, J. Cryst. Growth **532**, 125426 (2020).
[49] J. M. Ok, S. Yoon, A. R. Lupini, P. Ganesh, A. Huon, M. F. Chisholm, and H. N. Lee, ACS Appl. Mater. Interfaces **13**, 22059–22064 (2021).
[50] T. Harada, Unpublished results.
[51] D. J. Hagen, J. Yoon, H. Zhang, B. Kalkofen, M. Silinskas, F. Börrnert, H. Han, and S. S. P. Parkin, Adv. Mater. Interfaces **9**, 2200013 (2022).
[52] P. W. Tasker, J. Phys. C: Solid State Phys. **12**, 4977–4984 (1979).
[53] C. M. Yim, D. Chakraborti, L. C. Rhodes, S. Khim, A. P. Mackenzie, and P. Wahl, Sci. Adv. **7**, eabd7361 (2021).
[54] H. B. Michaelson, J. Appl. Phys. **48**, 4729 (1977).
[55] T. Harada, S. Ito, and A. Tsukazaki, Sci. Adv. **5**, eaax5733 (2019).
[56] T. Harada and A. Tsukazaki, APL Mater. **8**, 041109 (2020).
[57] T. Harada and A. Tsukazaki, Appl. Phys. Lett. **116**, 232104 (2020).
[58] C. Noguera, J. Phys.: Condens. Matter **12**, R367–R410 (2000).
[59] T. Higuchi and H. Y. Hwang, in *Multifunctional Oxide Heterostructures*, edited by E. Y. Tsymbal, E. R. A. Dagotto, C. B. Eom, and R. Ramesh (Oxford University Press, 2012), pp. 183–213.
[60] K. Kim, H. C. Choi, and B. I. Min, Phys. Rev. B **80**, 035116 (2009).
[61] J. H. Lee, T. Harada, F. Trier, L. Marcano, F. Godel, S. Valencia, A. Tsukazaki, and M. Bibes, Nano Lett. **21**, 8687–8692 (2021).
[62] F. Trier, P. Noël, J.-V. Kim, J.-P. Attané, L. Vila, and M. Bibes, Nat. Rev. Mater. **7**, 258–274 (2021).
[63] J. D. Sau, R. M. Lutchyn, S. Tewari, and S. D. Sarma, Phys. Rev. Lett. **104**, 040502 (2010).
[64] A. Yamakage, Y. Tanaka, and N. Nagaosa, Phys. Rev. Lett. **108**, 087003 (2012).
[65] M. F. Crommie, C. P. Lutz, and D. M. Eigler, Nature **363**, 524–527 (1993).
[66] Y. Hasegawa and P. Avouris, Phys. Rev. Lett. **71**, 1071 (1993).

© Author(s) 2022

[67]J. E. Hoffman, K. McElroy, D.-H. Lee, K. M. Lang, H. Eisaki, S. Uchida, and J. C. Davis, Science **297**, 1148–1151 (2002).
[68]T. Zhang, P. Cheng, X. Chen, J.-F. Jia, X. Ma, K. He, L. Wang, H. Zhang, X. Dai, Z. Fang, X. Xie, and Q.-K. Xue, Phys. Rev. Lett. **103**, 266803 (2009).
[69]P. Roushan, J. Seo, C. V. Parker, Y. S. Hor, D. Hsieh, D. Qian, A. Richardella, M. Z. Hasan, R. J. Cava, and A. Yazdani, Nature **460**, 1106–1109 (2009).
[70]B. Jäck, Y. Xie, B. Andrei Bernevig, and A. Yazdani, Proc. Natl. Acad. Sci. U. S. A. **117**, 16214–16218 (2020).
[71]P. Kong, G. Li, Z. Yang, C. Wen, Y. Qi, C. Felser, and S. Yan, arXiv:2111.10062 (2021).
[72]F. Mazzola, C.-M. Yim, V. Sunko, S. Khim, P. Kushwaha, O. J. Clark, L. Bawden, I. Marković, D. Chakraborti, T. K. Kim, M. Hoesch, A. P. Mackenzie, P. Wahl, and P. D. C. King, npj Quantum Mater. **7**, 20 (2022).
[73]S. E. Barnes, J. I. Ieda, and S. Maekawa, Sci. Rep. **4**, 4105 (2014).
[74]O. Krupin, G. Bihlmayer, K. Starke, S. Gorovikov, J. E. Prieto, K. Döbrich, S. Blügel, and G. Kaindl, Phys. Rev. B **71**, 201403 (2005).
[75]R. Wiesendanger, Rev. Mod. Phys. **81**, 1495 (2009).
[76]C. Hanneken, F. Otte, A. Kubetzka, B. Dupé, N. Romming, K. von Bergmann, R. Wiesendanger, and S. Heinze, Nat. Nanotechnol. **10**, 1039–1042 (2015).
[77]M. Bode, S. Heinze, A. Kubetzka, O. Pietzsch, X. Nie, G. Bihlmayer, S. Blügel, and R. Wiesendanger, Phys. Rev. Lett. **89**, 237205 (2002).
[78]Y. Yasui, C. J. Butler, N. D. Khanh, S. Hayami, T. Nomoto, T. Hanaguri, Y. Motome, R. Arita, T.-h. Arima, Y. Tokura, and S. Seki, Nat. Commun. **11**, 5925 (2020).
[79]V. Eyert, R. Frésard, and A. Maignan, Chem. Mater. **20**, 2370–2373 (2008).
[80]K. I. Bolotin, K. J. Sikes, Z. Jiang, M. Klima, G. Fudenberg, J. Hone, P. Kim, and H. L. Stormer, Solid State Commun. **146**, 351–355 (2008).
[81]L. Banszerus, M. Schmitz, S. Engels, M. Goldsche, K. Watanabe, T. Taniguchi, B. Beschoten, and C. Stampfer, Nano Lett. **16**, 1387–1391 (2016).
[82]R. O. Dillon, I. L. Spain, J. A. Woollam, and W. H. Lowrey, J. Phys. Chem. Solids **39**, 907–922 (1978).
[83]D. D. L. Chung, J. Mater. Sci. **37**, 1475–1489 (2002).
[84]N. García, P. Esquinazi, J. Barzola-Quiquia, B. Ming, and D. Spoddig, Phys. Rev. B **78**, 035413 (2008).
[85]L. Pfeiffer, K. W. West, H. L. Stormer, and K. W. Baldwin, Appl. Phys. Lett. **55**, 1888 (1989).
[86]V. Umansky, M. Heiblum, Y. Levinson, J. Smet, J. Nübler, and M. Dolev, J. Cryst. Growth **311**, 1658–1661 (2009).
[87]T. M. Lu, D. C. Tsui, C.-H. Lee, and C. W. Liu, Appl. Phys. Lett. **94**, 182102 (2009).
[88]J. Falson and M. Kawasaki, Rep. Prog. Phys. **81**, 056501 (2018).
[89]I. P. Smorchkova, L. Chen, T. Mates, L. Shen, S. Heikman, B. Moran, S. Keller, S. P. DenBaars, J. S. Speck, and U. K. Mishra, J. Appl. Phys. **90**, 5196–5201 (2001).
[90]M. J. Manfra, K. W. Baldwin, A. M. Sergent, R. J. Molnar, and J. Caissie, Appl. Phys. Lett. **85**, 1722–1724 (2004).
[91]F. Trier, K. V. Reich, D. V. Christensen, Y. Zhang, H. L. Tuller, Y. Chen, B. I. Shklovskii, and N. Pryds, Appl. Phys. Lett. **111**, 092106 (2017).
[92]N. Koirala, M. Brahlek, M. Salehi, L. Wu, J. Dai, J. Waugh, T. Nummy, M.-G. Han, J. Moon, Y. Zhu, D. Dessau, W. Wu, N. P. Armitage, and S. Oh, Nano Lett. **15**, 8245–8249 (2015).
[93]S. M. Sze and K. K. Ng, *Physics of Semiconductor Devices* (Wiley, Hoboken, 2006).
[94]K. Jacobi, G. Zwicker, and A. Gutmann, Surf. Sci. **141**, 109–125 (1984).
[95]S. Y. Davydov, Semiconductors **41**, 696–698 (2007).
[96]S.-C. Lin, C.-T. Kuo, X. Liu, L.-Y. Liang, C.-H. Cheng, C.-H. Lin, S.-J. Tang, L.-Y. Chang, C.-H. Chen, and S. Gwo, Appl. Phys. Express **5**, 031003 (2012).
[97]S. J. Pearton, J. Yang, P. H. Cary IV, F. Ren, J. Kim, M. J. Tadjer, and M. A. Mastro, Appl. Phys. Rev. **5**, 011301 (2018).
[98]M. Mohamed, K. Irmscher, C. Janowitz, Z. Galazka, R. Manzke, and R. Fornari, Appl. Phys. Lett. **101**, 132106 (2012).
[99]K. G. Crawford, I. Maini, D. A. Macdonald, and D. A. J. Moran, Prog. Surf. Sci. **96**, 100613 (2021).
[100]F. Maier, J. Ristein, and L. Ley, Phys. Rev. B **64**, 165411 (2001).

© Author(s) 2022